Automatic Tuning for Sensorless Commissioning of Synchronous Reluctance Machines Augmented with High Frequency Voltage Injection

Publisher copyright

(Article begins on next page)

04 August 2020

Automatic Tuning for Sensorless Commissioning of Synchronous Reluctance Machines Augmented with High Frequency Voltage Injection

Paolo Pescetto, *Student Member, IEEE*, and Gianmario Pellegrino, *Senior Member, IEEE*

Abstract—Sensorless control of synchronous reluctance motors relies on the knowledge of the machine current-to-flux maps. Previous work demonstrated the feasibility of sensorless identification of the flux maps, performed by exciting the machine with square-wave voltage pulses at standstill, and without the need of rotor locking. The rotor position was initially estimated and then used throughout the identification, in open-loop fashion. In some cases, rotor oscillation and eventually position drift led to stop the identification before the programmed dq current domain was covered entirely. In this paper, the rotor position is closed-loop tracked during the motor commissioning to counteract the occurrence of rotor movement. The hysteresis-controlled excitation voltage is augmented with an high-frequency square-wave voltage component, and the position is tracked through demodulation of the current response to such high-frequency component. The proposed approach is experimentally verified on a 2.2 kW synchronous reluctance motor prototype. The results show that the i_d, i_q commissioning domain is substantially extended, resulting in more accurate flux maps. Moreover, self-tuning of the method is addressed and possible causes of error are analyzed and commented.

Index Terms—Magnetic Model Identification; Self-Commissioning; Synchronous Reluctance Motor; Flux Maps; Magnetization Curves; HF injection.

I. Introduction

SYNCHRONOUS Reluctance Motor (SyRM) drives are an attractive solution for replacing traditional Induction Motors (IM) variable speed drives in a wide number of applications, thanks to their high efficiency and competitive torque per volume ratio. Many industry applications demand for sensorless operation, either for cost or fault tolerance reasons. The inherently salient structure of SyRMs makes them suitable for low and zero speed sensorless control, but all the techniques present in the literature [1]- [3] require the knowledge of the current-to-flux machine characteristics, also called flux maps. This is a demanding issue due to the relatively complex magnetic structure of SyRMs, resulting in highly non-linear saturation and cross-saturation characteristics.

The test procedures for accurate evaluate the flux maps of SyRMs rely on dedicated test rigs and position transducer, like the one in [4], so they are not suitable for a full sensorless approach. Several automatic self-commissioning techniques were recently proposed for synchronous drives [5]- [9]. Yet, most of them require additional hardware and position transducers.

Work [10] described a square-wave voltage excitation technique for interior permanent magnet machines with encoder using pulses of low per unit value and requiring to lock the rotor. This technique was then improved by [11]- [12]

specifically for SyRM by introducing high test voltage and avoiding the use of position transducer. The improved method, performed at standstill, resulted accurate and robust towards stator resistance detuning even when in free-shaft condition, which is the worst-case scenario for standstill self-commissioning. Plus, it is encoderless. In [11]- [12], only the initial rotor position is estimated before the test, either through High Frequency (HF) injection techniques or imposing it through DC current excitation. Then, the position is considered constant during the test, but the machine response to the excitation may cause undesired rotor movement, thus making the initial position estimation inaccurate. The rotor can even start spinning and the test would fail. This shortcoming limits the feasible measurement area in the dq current plane.

This work follows what recently presented in [13], where the flux map identification was augmented by HF voltage injection, for online estimation of the rotor position. In this way, the dq axes position is tracked in real time, considerably reducing the risk of rotor movement and test failure. The additional contributions of this extended version of [13] are:

1) A new and more reliable feedback error signal is introduced, permitting to stop the d and q current test (test #3) automatically, without a position transducer. In the conference paper an encoder was still required to stop test #3.
2) Sensitivity analysis of the self-commissioning results respect to inaccurate parameter estimation is given, to prove the robustness of the method.
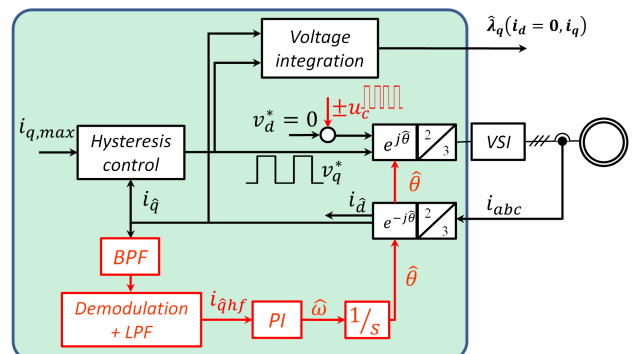3) An automatic calibration procedure of the commissioning test is suggested.

Fig. 1. Block diagram of drive controller configuration used for test #2. The red blocks are added only if HF tracking loop is adopted.

In turn, this paper proposes a full sensorless self commissioning technique capable of accurate identification of the SyR motor flux maps. The area explored in the i_d, i_q domain was enlarged, the accuracy of the flux curves was improved respect to the previous version with open-loop position estimation and the test was made more stable than before, permitting to store a higher number of points per session.

The paper provides a detailed theoretical analysis, supported by experimental validation on a 2.2 kW SyRM prototype.

II. PROPOSED SELF-COMMISSIONING METHOD

In [11] and [12], the motor is excited at standstill with square wave voltage pulses with amplitude compatible with the rated voltage and the stator flux linkage is evaluated through voltage integration. The knowledge of the rotor position comes from initial sensorless estimation, and requires that the rotor does not change its position upon the flux map commissioning. All tests reported in the paper refer to free-shaft conditions. If, otherwise, the mechanical load is connected, this can help keeping the rotor standstill facilitating the commissioning.

A. Review of the Flux Identification Method

The procedure is divided in three stages, to evaluate the flux along d axis, along q axis and the dq cross-saturation effect, respectively. In **test #1**, the reference voltage in d-axis v_d^* is a square wave whose polarity is reversed when the current i_d exceeds a predefined threshold value $i_{d,max}$, after an hysteresis controller. Meanwhile, v_q^* is set to zero and negligible i_q is expected. In this first test, the flux linkage characteristic along the d-axis λ_d can be estimated as:

$$\widehat{\lambda}_d(i_d, i_q) = \int (v_d - R_s i_d) dt \qquad (1)$$

Where v_d is estimated basing on inverter voltage commands after nonlinear effects compensation, R_s is the stator resistance and $i_q = 0$.

Then, a dual test is run on the q-axis (**test #2**). The reference voltage v_q^* is a square wave while $v_d^* = 0$. Again, v_q is estimated basing on inverter voltage commands while $i_d = 0$. The magnetic curve along q-axis direction can be evaluated:

$$\widehat{\lambda}_q(i_d, i_q) = \int (v_q - R_s i_q) dt \qquad (2)$$

Finally, **test #3** evaluates the cross-saturation effect. The d and q axes are excited at the same time, again with a square wave voltage, and the polarity in each axes is reversed when the respective current exceeds the $i_{d,max}$ or $i_{q,max}$ value. Equations (1) and (2) can be used to evaluate the stator flux linkage in the whole measurement domain. Details can be found in [12].

B. Open-Loop Position Estimation

In [12] the rotor position was sensorless evaluated before the self-commissioning test, either through saliency based techniques or aligning the rotor along a defined direction.

Provided that the initial position estimate is correct, tests #1 and #2 should inherently mantain the standstill condition and keep the initial alignment throughout the test, since none of the d or q axes, excited alone, might produce torque. Unfortunately, this is true only for the d axis, whereas during test #2 minimal misalignments of the excitation from the actual q axis tends to produce transient torque and movement. Therefore, test #2 tends to be unstable. Dealing with test #3, this inherently involves high transient torque values, as both axes are excited: the respect of the standstill condition thus requires that the torque polarity is reversed quickly enough not to produce substantial movement.

The results of [12] showed that the approach based on the estimate of the initial position works properly for test #1, where position errors produce a torque that realings the rotor d axis to the $\widehat{d}$ excitation direction. Conversely, for test #2 the misalignment torque tends to move the rotor away from the initial position, and eventually make it spinning. This trend has to do with the amplitude of the current sweep $i_{q,max}$. In turn, the q axis identification session widhstood sudden failures, very often before the i_q axis was explored in its entirety. Similarly, in test #3 the rotor might rotate if the current limits $i_{d,max}$, $i_{q,max}$ are excessive, or if they are combined in a way that torque reversals are not fast enough.

In turn, loss of the initial rotor position limits the measurement area along the q-axis both in tests #2 and #3. Fixing the misalignment and spin off problems is the scope of this paper.

C. Sensorless Online Position Tracking

To avoid shaft rotation and dq misalignment, previous work [13] proposed to estimate the rotor position online, during the self-cmmissioning procedure, for tests #2 and #3.

As the machine is at standstill, a saliency based position tracking loop is necessary. Saliency-based self-sensing techniques are widely used for sensorless control of torque and speed, and they differ from one another for the type of injected signal and the demodulation algorithm. In this work, the rectangular pulsating injection proposed in [14] is adopted. An HF voltage u_c is injected in the estimated $\widehat{d}$-axis at half of the switching frequency ($f_{sw} = 10\ kHz$, $f_{HF} = 5\ kHz$), superimposed to the hysteresis driven test voltage.

$$u_c(k) = -u_c(k-1) \qquad (3)$$

In turn, both the HF and flux excitation voltage components are square waves. To avoid confusion, the amplitudes of the hysteresis square wave voltage will be called $V_{test,d}$ and $V_{test,q}$, while the amplitude of the HF voltage injected for position tracking will be referred to as u_c, as said. The HF current response in the estimated $\widehat{q}$-axis is demodulated, obtaining the position error signal $i_{\widehat{q}hf}$, which is forced to zero through a PLL as shown in Fig. 1:

$$i_{\widehat{q}hf} = \frac{|u_c|(L_d - L_q)}{4\omega_c L_d L_q} sin(2\Delta\theta) \cong k_\epsilon \cdot \Delta\theta \qquad (4)$$

$$k_\epsilon(i_d, i_q) = \frac{|u_c|(L_d - L_q)}{2\omega_c L_d L_q} \qquad (5)$$

where L_d, L_q are differential inductances in dq axis and ω_c is the angular frequency of the injected HF voltage. Because of magnetic saturation, k_ϵ depends on (i_d, i_q). Fig. 1 shows the

control scheme for test #2. The scheme for test #3 is identical, but the hysteresis regulators of both axes are activated.

The choice of the $5\ kHz$ injection frequency permits the maximum possible decoupling between the signals related to the flux identification and the ones for position tracking. Moreover, it was demonstrated in [13] that such HF component does not affect the flux estimation in (1),(2). Unfortunately, this sensorless technique will suffer for position error due to cross-saturation effect [15], not considered in (4). The cross-saturation effect can be compensated, [15], [16], but the correction would require the knowledge of the machine flux maps, which is not available at this stage.

III. AUTOMATIC TUNING PROCEDURE

A. Current Limits $i_{d,max}$ and $i_{q,max}$

The threshold current limits during self-commissioning test define the area in the dq plane where the flux maps are evaluated. A large measurement domain is usually desired, however if the current limits are set too high the success of the test can be compromised in presence of position estimation error, as mentioned in section II-B.

As said, the d-axis test #1 is self aligning, so the threshold value $i_{d,max}$ can be set as high as desired (20 A here, for a 7 A(pk) machine). Conversely, the $i_{q,max}$ limit of test #2 directly influences the misalignment torque, and the test fails if the threshold value is set too high. Previous works [11] [12] used a fixed value for $i_{q,max}$, obtained by trial and error. In this paper it is suggested to increase $i_{q,max}$ ramp-wise, starting from zero, and stop the test when a rotor movement is detected, as detailed in the next section. The slope of the ramp must be as slow as possible, and the final target $i_{q,max}$ can be set equal to $i_{d,max}$, but it is never reached, if the rotor shaft is free. Similarly, during test #3 torque is naturally produced and the current limits $i_{d,max}$ and $i_{q,max}$ define the maximum torque amplitude. Also in this case, the current in $\widehat{d}$-axis tends to align

the rotor to the estimated position, while $i_{\widehat{q}}$ is destabilizing. Therefore, this paper suggests to use a fixed value for $i_{d,max}$ and ramp the $i_{q,max}$ limit, again stopping the test when a relevant movement is detected. This technique guarantees the maximum possible exploration of the dq current plane.

B. Automatic Stop of test#2

Detection of unwanted rotor movement is necessary to stop data collection during tests #2 and #3, in case the rotor starts rotating. During test #2, it is expected that the current component on the other axis $i_{\widehat{d}}$ is zero, as the $\widehat{q}$-axis is excited. Any rotor misalignment causes $i_{\widehat{d}} \neq 0$. Therefore, the amplitude of $i_{\widehat{d}}$ is used as error feedback. As suggested in [17] the test #2 will be stopped when $i_{\widehat{d}}$ overcomes a predefined value.

C. Automatic Stop of test#3

When both axes are excited, [17] proposed a movement detection feedback by observing whether the $i_{\widehat{d}}$ is monotonic between one voltage reversal and the next one, which is what would be expected according to the constant applied voltage pulse $v_{\widehat{d}=\pm V_{test,d}}$. The $i_{\widehat{d}}$ occurrs to be non monotonic when the position error is significant, and this information was usefully exploited to stop the test before the rotor started rotating. At each sampling time, the movement detection signal mov is increased by one if the $i_{\widehat{d}}$ derivative does not respect the sign of the applied $v_{\widehat{d}}$, according to (6). The movement detection feedback is reset to zero after each half cycle of the $v_{\widehat{d}}$.

$$mov(k) = mov(k-1) + \frac{1 - sign\left[(i_{\widehat{d}}(k) - i_{\widehat{d}}(k-1)) \cdot v_{\widehat{d}}(k)\right]}{2}$$
(6)

In this formulation, the sign of the derivative of $i_{\widehat{d}}$ is evaluated as the sign of $(i_{\widehat{d}}(k) - i_{\widehat{d}}(k-1))$. This signal represents an approximation of the integral of the position error during one
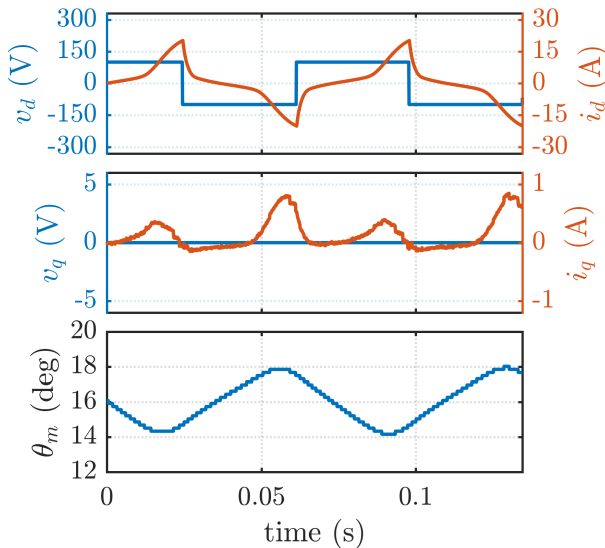

Fig. 2. Test #1 (experimental); $V_{test,d} = 100\ V$. From top to bottom: voltage and current in d-axis; voltage and current in q-axis; mechanical position.
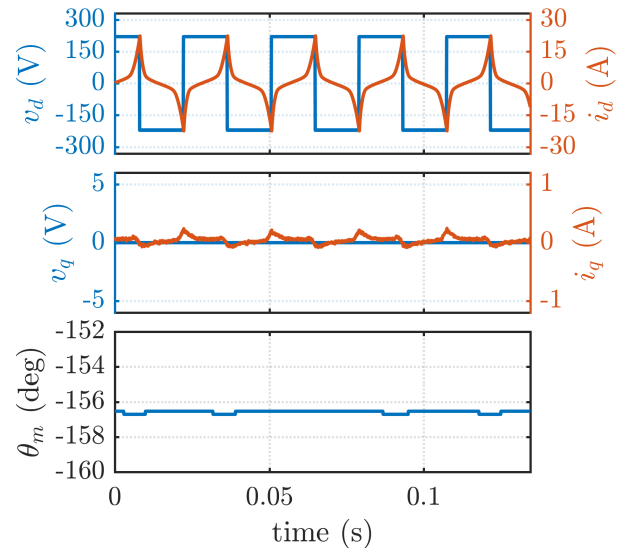

Fig. 3. Test #1 (experimental); $V_{test,d} = 200\ V$. From top to bottom: voltage and current in d-axis; voltage and current in q-axis; mechanical position.

sweep of the d-axis current. The test is stopped if the error signal (6) overcomes a defined threshold value. This technique resulted appropriate when the test is performed with open loop position estimation [17].

However, in presence of HF signal injection for online position tracking the one-step derivative $(i_{\hat{d}}(k) - i_{\hat{d}}(k-1))$ is affected by the superimposed HF component, causing false trigger of the stop function. Considering that the HF injection frequency is synchronized at half the sampling frequency, the movement detection signal was modified to:

$$mov(k) = mov(k-1) + \frac{1 - sign\left[\left(i_{\hat{d}}(k) - i_{\hat{d}}(k-2)\right) \cdot v_{\hat{d}}(k)\right]}{2} \tag{7}$$

where the current derivative is evaluated over the span of two current samples. With this new formulation, the movement detection feedback is increased by one at every sample time when the sign of $(i_{\hat{d}}(k) - i_{\hat{d}}(k-2))$ is not in accordance with the applied $v_{\hat{d}}$. The movement detection signal obtained with (6) and (7) are experimentally compared in Fig. 9 and 10.

D. Voltage Amplitudes $V_{test,d}, V_{test,q}$ and u_c

Previous works [17] demonstrated that the higher is the fundamental excitation voltage used in the tests, the lower is the effect of eventual inaccuracies in stator resistance estimation and compensation of inverter non-linear effects.

Moreover, high values of $V_{test,d}$ and $V_{test,q}$ correspond to a frequent current and torque reversal, during tests #2 and #3, and this makes the respect of the standstill condition easier. Therefore, both test #2 and #3 result more stable and accurate if the amplitude of the test voltage is maximized.

A possible drawback in using high $V_{test,d}$ and $V_{test,q}$ is that it can result in a reduced number of current (and flux) samples per period. In [17] it is suggested to perform the self-commissioning test with the maximum available voltage, according to inverter limitation V_{max}, and then repeat the test at reduced voltage amplitude if the umber of samples per period is not satisfactory.

Fig. 2 and 3 compare test #1 performed with a test voltage $V_{test,d} = 100\ V$ and the same test done with $V_{test,d} = 200\ V$. In both cases the rotor position was open loop estimated. As can be seen, higher test voltage brings lower position oscillations, lower undesired current in the not excited axis and so more accurate flux estimation. An analogous comparison for the q-axis test showed that test #2 was successfully performed using $V_{test,q} = 200\ V$ while it failed with $V_{test,q} = 100\ V$ because in this case the test was so unstable that the rotor moved from its initial position and it started to rotate.

If the commissioning test is augmented with online position tracking loop, injecting a high u_c gives a higher demodulated feedback and therefore the position tracking loop becomes more stable. Conversely, a high u_c poses limitations to the available test voltages $V_{test,d}$ and $V_{test,q}$. Therefore, the choice of test and HF voltage amplitudes are strictly related, and a trade-off is needed, considering the inverter dc-link voltage.

During test #2, the voltage vector touches the four vertex of a rectangle, in the v_d, v_q plane. The four points, represented in Fig. 4(a), are $v_d = \pm u_c$ and $v_q = \pm V_{test,q}$. In test #3 the
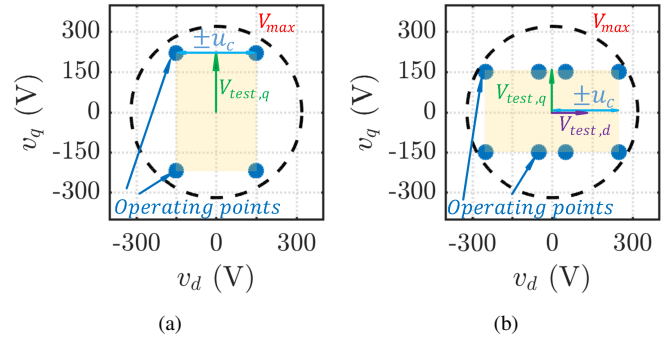

Fig. 4. Testing area for test #2 and #3 augmented with HF injection and inverter voltage limit $V_{max} = 320\ V$. a) test #2, $V_{test,q} = 220\ V$; $u_c = 150\ V$. b) test#3, $V_{test,d} = V_{test,q} = 150\ V$; $u_c = 100\ V$.

voltage vector touches 8 points, represented in Fig. 4(b). Such points are: $v_d = \pm V_{test,d} \pm u_c$; $v_q = \pm V_{test,q}$. Taking into account the inverter voltage limitation $V_{max} = v_{dc}/\sqrt{3}$, the following relations hold:

$$u_c < \begin{cases} \sqrt{V_{max}^2 - V_{test,q}^2} & \text{test \#2} \\ \sqrt{V_{max}^2 - V_{test,q}^2} - V_{test,d} & \text{test \#3} \end{cases} \tag{8}$$

E. Position Tracking Loop

The equivalent block diagram of the position tracking loop is represented in Fig. 5, where ω_f is the bandwidth of the demodulation low-pass filter shown in Fig. 1. Further details are available in [14]. The bandwidth of this position tracking loop will be called ω_b. Accurate tuning of the such tracking loop would require the preliminary knowledge of the machine flux maps, which is not available at this stage. Anyway, a rough preliminary estimation of the machine inductances is sufficient for automatic tuning, as will be detailed in the following.

For sensorless control, it is usually desired to increase ω_b as far as possible, in order to have a fast control response in transient conditions. Anyway, in the proposed self commissioning procedure, the rotor movement in test #2 and #3 can be seen as a slow drift from the initial position plus fast vibrations due to the sign variation in the test square wave voltage used for flux identification. The goal of the HF tracking loop is to update the rotor position in order to follow the drift, which is relatively slow, while it is not required to track the vibrations. Therefore, a low bandwidth sensorless control is sufficient (e.g. $\omega_b = 10 \div 20\ rad/s$), permitting poor tuning precision. A more performing sensorless technique based on the machine's flux maps, such as [16], can be adopted after the self-commissioning stage.
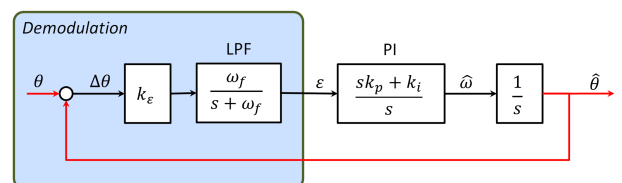

Fig. 5. Sensorless position tracking loop.

Once determined u_c according to the specifications detailed in Section III-D, the parameter k_ϵ (5) must be estimated, via a preliminary evaluation of the machine's differential inductances. The value of L_d can be obtained from test #1 which, as said, is stable and does not require HF injection. Test #2 performed at open loop is marginally stable, but gives enough information about L_q for tuning the position estimation loop. According to Fig. 5, the open loop transfer function between the observed and real position is:

$$H = k_\epsilon \frac{\omega_f}{s + \omega_f} \cdot \frac{s k_p + k_i}{s} \cdot \frac{1}{s} \tag{9}$$

Therefore, neglecting the integrative gain, the bandwidth of the position tracking loop is:

$$\omega_b = k_\epsilon k_p \tag{10}$$

This last relationship can be used to tune the parameter k_p, after the desired bandwidth value is defined. Afterwards, the integral gain k_i is calibrated considering that the frequency of the zero introduced by the PI regulator must be lower than the bandwidth, for the sake of keeping the phase margin of the tracking loop above 45°:

$$k_i < k_p \omega_b \tag{11}$$

Last, the frequency of the demodulation filter ω_f must be sufficiently higher than the bandwidth but lower than the injection frequency ω_c. The choice of injecting the HF signal at half of the switching frequency f_{sw} permits the highest possible frequency range for the tuning of ω_f and ω_b, therefore it facilitates the tuning procedure in absence of flux maps.

$$\omega_b \ll \omega_f \ll \omega_{sw} \tag{12}$$

In this implementation, the selected values are $\omega_b = 20\ rad/s$, $\omega_f = 940\ rad/s$ and $f_{sw} = 10\ kHz$.

IV. Data Fit and Sensitivity to Detuning

After the magnetic model identification tests are completed, it is necessary to manipulate the acquired data to obtain the flux characteristics in an appropriate form usable for controlling the SyRM drive. For example, the flux maps can be implemented in form of look up tables or, alternatively, using analytical functions. The polynomial magnetic model presented in [12] is based on few parameters and was successfully tested on SyRMs of different size. For this reason it will be used also in this work.

Incorrect parameters estimation can affect the flux estimation in (1) and (2). This section analyzes and quantifies the inaccuracy introduced by such error sources, showing that the method is not sensitive to inaccurate estimates of the stator resistance and the inverter voltage drop.

A. Polynomial Model

The model is based on the following equations:

$$i_d = \lambda_d \left(a_{d0} + a_{dd}\lambda_d^S + \frac{a_{dq}}{V+2}\lambda_d^U \lambda_q^{V+2} \right) \tag{13}$$

$$i_q = \lambda_q \left(a_{q0} + a_{qq}\lambda_q^T + \frac{a_{dq}}{U+2}\lambda_d^{U+2}\lambda_q^V \right) \tag{14}$$

The exponents can be fixed according to TABLE II, while the coefficients a_{d0}, a_{dd}, a_{q0}, a_{qq} and a_{dq} can be found through iterative linear least square procedure. In particular, a_{d0} and a_{dd} are obtained from test #1, a_{q0} and a_{qq} from test #2 and a_{dq} from test #3. Details can be found in [12].

B. Stator Resistance Estimation

The stator resistance parameter is used in (1) and (2) to compensate for the resistive voltage drop. The value of R_s is measured before the commissioning test by injecting dc current in d-axis and its detuning is mostly due to temperature effects. During the flux identification test, the windings are excited with high per-unit current but the winding temperature is hardly changing due to the limited duration of the test (a few seconds). Therefore, detuning of R_s is negligible. Nevertheless, in case the stator resistance is not estimated accurately, such error produces a flux estimation error $\epsilon_{\lambda,Rs}$:

$$\epsilon_{\lambda,Rs} = \left(\widehat{R}_s - R_s \right) \int i_d dt \tag{15}$$

The main effect of resistance estimation error $\widehat{R}_s - R_s$ is that the amplitude of the loop described by $\lambda_d(i_d)$ estimated characteristic increases. Fig. 6(a) shows the case of 100 % detuning ($\widehat{R}_s = 0$). As can be seen, even in this extreme case the mean between the upper and lower curves of the detuned flux characteristic (black line) is very close to the red loop, where the resistive voltage drop was correctly compensated.

It must be remarked that, because of the absence of PM, the variability of R_s is the only effect of temperature variation. Therefore, the high robustness against inaccurate stator resistance estimation also corresponds to high robustness against temperature variation.

C. Inverter Non-linearities Compensation

Similarly, inaccurate compensation of inverter non-linear effect directly produces a flux estimation error $\epsilon_{\lambda,Vth}$:

$$\epsilon_{\lambda,Vth} = \int \left(\widehat{V}_{th} - V_{th} \right) \cdot sign\left(i_d \right) dt \tag{16}$$

where $\widehat{V}_{th}$ and V_{th} are the estimated and real amplitude of the inverter distortion voltage [18]. If a constant V_{th} is considered,
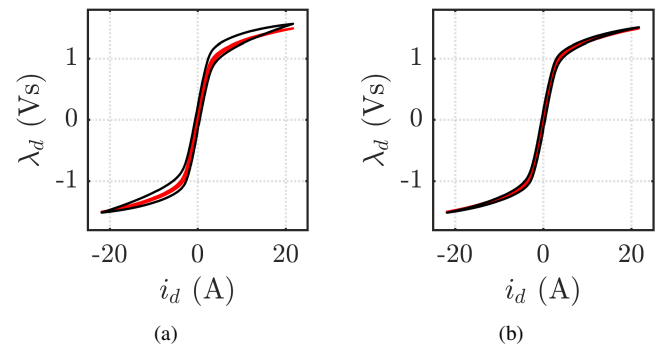

Fig. 6. a) Estimated $\lambda_d(i_d,0)$ characteristic with (red) and without (black) compensating the resistive voltage drop; b) Estimated $\lambda_d(i_d,0)$ characteristic with (red) and without (black) compensating inverter non-linear effect V_{th}.

the flux error would be a triangular time waveform [17]. Similarly to $\epsilon_{\lambda,Rs}$, the eventual error $\epsilon_{\lambda,Vth}$ increases the thickness of the loop in the estimated flux characteristic, but without considerably varying its average value. Fig. 6(b) compares the flux computed with accurate inverter compensation (red line) with the case of 100 % detuning (black line).

D. Discussion

Because of magnetic saturation, the time waveform of $\epsilon_{\lambda,Rs}$ is highly nonlinear, whereas $\epsilon_{\lambda,Vth}$ is approximately a triangular waveform. For this reason, it is not obvious to evaluate which of the two terms might affect more the flux estimation in a self-commissioning test. Different scenarios are possible depending on the accuracy of $\widehat{R}_s$ and $\widehat{V}_{th}$.

For the drive under test, the peak value of the two error terms is compatible (around 0.1 Vs), but $\epsilon_{\lambda,Rs}$ has higher effect on the loop thickness because of its different time waveform. It must be considered that the case of 100% detuning of $\widehat{R}_s$ presented in Fig. 6(a) is an hyper worst case scenario, since it is very unlikely that in real applications the resistance is completely unknown. More reasonably, R_s can be uncertain (i.e. known at the wrong temperature), so the discrepancy of the observed flux would be much lower than in Fig. 6(a). In conclusion, the higher is the amplitude of the applied voltage, the lower will be the sensitivity of the magnetic curves to both the detuning of $\widehat{R}_s$ and $\widehat{V}_{th}$.

V. EXPERIMENTAL RESULTS

The proposed square-wave injection self-identification technique augmented by HF signal injection was experimentally tested on a 2.2 kW SyRM. TABLE I. summarizes the main machine characteristics. A dSPACE 1103 PPC controller board was used for the experiments.

A. Flux maps identification

As said, test #1 is stable using the open loop position estimate approach, therefore this was done without HF injection.

Nominal current [A]	5.08
Nominal voltage [V]	400
Pole pairs	2
Nominal torque [Nm]	15
Nominal speed [rpm]	1400
Nominal power [kW]	2.2
Phase resistance [Ω]	3.58
Switching frequency [kHz]	10
Number of turns/phase	159

Tests #2 and #3 were performed both with and without HF injection, for the sake of comparison.

Fig. 7 and Fig. 8 compare the time waveforms of voltages and currents in test #2. In both cases, the $i_{q,max}$ limit was progressively increased and the test was stopped when relevant i_d was detected, according to the stop criterion described in Section III-B. In Fig. 7, a voltage amplitude $V_{test,q} = 200\ V$ was applied and the q current reaches a maximum swing of 7.9 A peak. Fig. 8 refers to the same test with HF injection and position estimation. The injected HF voltage u_c was 150 V, the demodulation low-pass filter was set at 150 Hz and the test voltage $V_{test,q}$ was 220 V. From the comparison, it is clear that thanks to the HF position tracking loop the measurement range is considerably improved, since the q current swing increased from 7.9 A up to 13.2 A peak (+67 %).

Fig. 9 and Fig. 10 refer to test #3, again comparing the two situations with and without HF signal injection. Also in this case, the $i_{q,max}$ limit was progressively increased, while the $i_{d,max}$ range was kept constant to 20 A. In Fig. 9 the adopted test voltages are $V_{test,d} = V_{test,q} = 200\ V$. In Fig. 10, the injected voltage is $u_c = 100\ V$, the cut-off frequency of the demodulation LPF is 50 Hz and the test voltage $V_{test,d} = V_{test,q} = 150\ V$. From the comparison it is evident that, using the same $i_{d,max}$ limit, the $i_{q,max}$
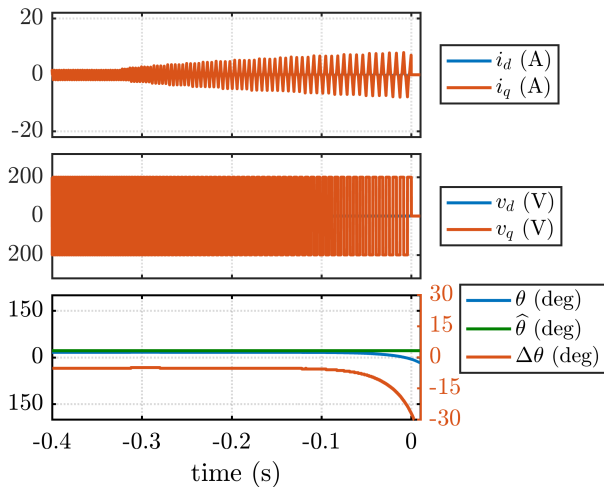

Fig. 7. Test #2 without HF injection. From top to bottom: currents in dq axes; applied voltages; measured and observed angle and and position error. $V_{test,q} = 200\ V$.
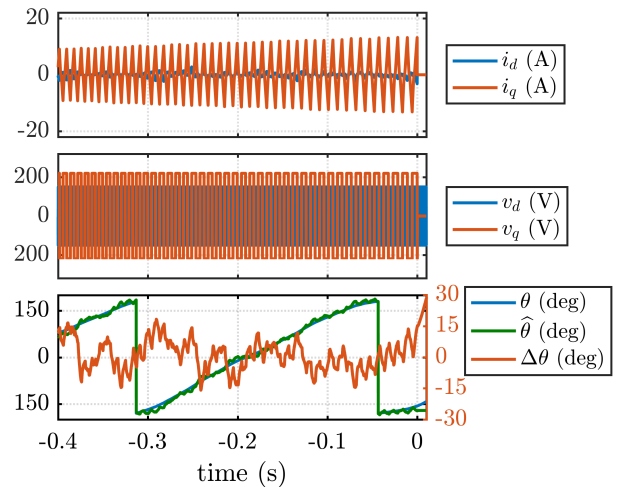

Fig. 8. Test #2 with HF injection. From top to bottom: currents in dq axes; applied voltages; measured and observed angle and and position error. $V_{test,q} = 220\ V$, $u_c = 150\ V$.
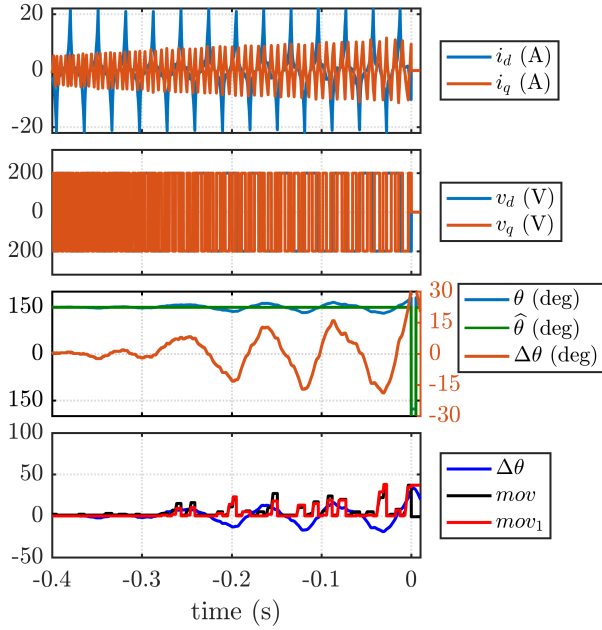
Fig. 9. Test #3 without HF injection. From top to bottom: currents in dq axes; applied voltages; measured and observed angle and and position error. $V_{test,d} = V_{test,q} = 200\ V$.
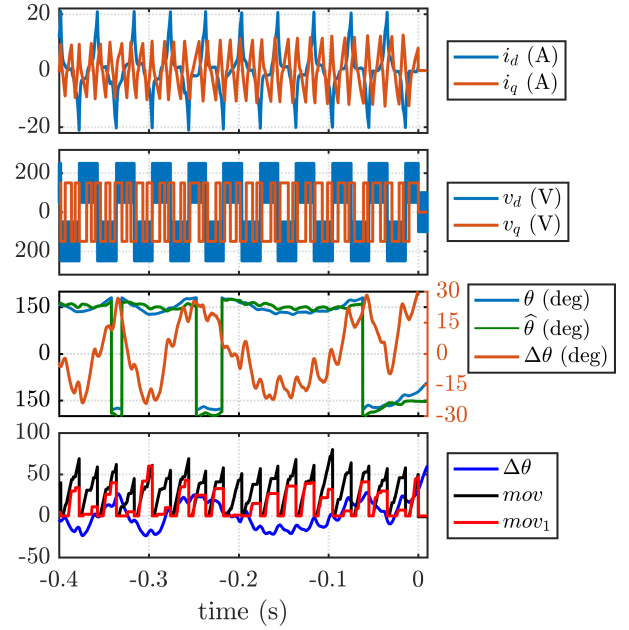

Fig. 10. Test #3 with HF injection. From top to bottom: currents in dq axes; applied voltages; measured and observed angle and and position error. $V_{test,d} = V_{test,q} = 150\ V$, $u_c = 100\ V$.

range is marginally improved from 11.5 A to 12.6 A. The limited improvement of the measurement domain for test #3 can be explained considering that during this test both axes are excited, so torque is inherently produced. Therefore, regardless the technique adopted for position estimation, for higher current the torque caused relevant position oscillations, arming the stability of the test. Anyway it must be remarked that more than three times the rated current was reached.

The bottom plot in Fig. 9 and 10 compares the position error, the movement detection signal calculated according to (6) and the one obtained with (7). The three signals are respectively called $\Delta\theta$, mov and mov_1 in the plot. As can be seen, the two position error feedback are equivalent when the test #3 is performed at open loop, but they are considerably different if online position tracking is adopted. Indeed, in this case the function obtained with (6) is not reliable as position error feedback, since it grows up to approximately the same value at every sweep of i_d despite the position error is big or not. Conversely, the amplitude of signal mov_1 at the end of one sweep of i_d is approximately proportional to $\Delta\theta$. Therefore, this signal can be used as stop criteria. It must be noted that, since the current follow a random trajectory in the dq plane, the produced position error is partially aleatory, so the test can be prematurely stopped even using the feedback mov_1. In this case it is necessary to repeat the test.

The trajectories covered during the three tests in the dq current plane are summarized in Fig. 11, comparing the case with (subfigure a) or without (subfigure b) HF signal injection and position estimation. It is demonstrated that the position tracking increases the stability of tests #2 and, limitedly, #3, so improving the current domain of the identification. As can be seen, the domain of all the test #1, #2 and #3 are extended to strong saturation and cross-saturation conditions.

B. Flux Curves

Referring to the polynominal model (13), (14), optimal values of a_{d0} and a_{dd} were conveniently obtained after test #1 performed at open loop. Different sets of values for a_{q0}, a_{qq} and a_{dq} were calculated from the results of test #2 and test #3
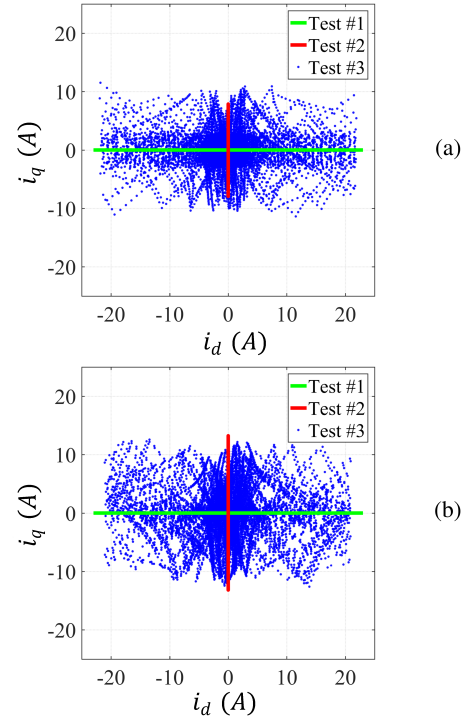

Fig. 11. Achievable measurement area in the current plane for test #1, #2 and #3 using open loop using (a) open loop position estimation; (b) HF tracking loop. Green: test #1; Red: test #2; Blue: test #3.

performed with and without closed-loop position estimation. TABLE II reports the parameters obtained in the two cases.

C. Results for test #2

The magnetic curve resulting from test #2 is shown as solid lines in Fig. 13, where the blue curves are the reference model, obtained with the constant speed method, the red lines are obtained with open loop position estimation and the green ones with HF injection. The saturation characteristic obtained at open loop well represents the reference line up to roughly 8 A, i.e. within the current swing that was explored during the identification. However, the deviation from the reference model is large for higher current values (overload conditions). On the other hand, the flux characteristic obtained exploiting the HF injection is well in accordance with the reference up to 15÷18 A, thanks to the extended measurement range.

D. Results for test #3

The results of the LLS fitting procedure based on test #3 are shown in Fig. 12 and Fig. 13. The same color conventions were adopted for the two figures. Solid lines represent the flux characteristic in each axis when the current in the other axis is null, while the dotted lines are the flux curves in presence of strong cross-saturation effect. In Fig. 12, $i_d(\lambda_d, \lambda_q = 0)$ curves obtained in the three cases are well superimposed. Conversely, the $i_d(\lambda_d, \lambda_q = 0.6)$ curve is more accurate when obtained from the open loop test (red curves) rather than using HF injection. Therefore, the small increase of the measurement area in test #3 obtained using HF injection did not help improving the cross-saturation evaluation accuracy.

Looking at Fig. 13, the $i_q(\lambda_d = 0, \lambda_q)$ and $i_q(\lambda_d = 1.2, \lambda_q)$ curves are better represented when the HF injection is adopted. The red curves suffer from the error on the q-axis self-characteristic obtained in test #2 (parameters a_{q0} and a_{qq}), even if the cross-saturation term a_{dq} evaluated in test #3 may be more accurate than the one used for the green lines.

TABLE III summarizes the suggested testing sequence for the full characterization of the flux maps. It is suggested to **use the HF injection to improve test #2, and not to use it during test #3**, which showed to better perform at open loop.

E. Response of Sensorless Control

As proof of concept, the SyRM under test is controlled using the sensorless control technique presented in [16] and the flux curves coming from the self-commissioning. The rotor position observer uses the active flux concept, augmented with high-frequency voltage injection in the low speed and zero
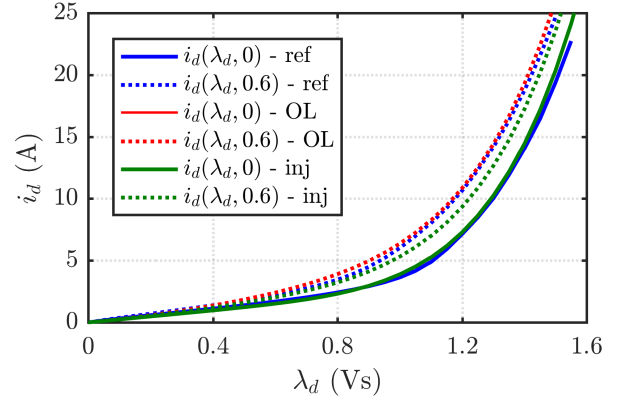

Fig. 12. $i_d(\lambda_d, \lambda_q)$ saturation characteristic obtained after LLS fitting procedure. Blue: reference curve; Red: test #3 with open loop position estimation; Green: test #3 with position tracking loop. Solid lines: $\lambda_q = 0\ Vs$; dotted lines: $\lambda_q = 0.6\ Vs$ (strong cross-saturation)
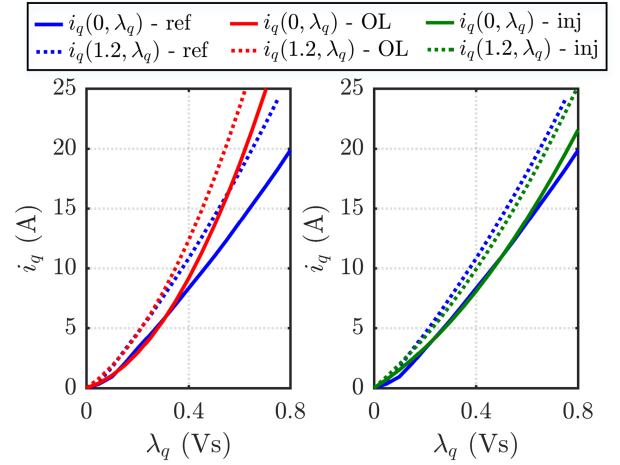

Fig. 13. $i_q(\lambda_d, \lambda_q)$ saturation characteristic obtained after LLS fitting procedure. Blue: reference curve; Red: test #3 with open loop position estimation; Green: test #3 with position tracking loop. Solid lines: $\lambda_d = 0\ Vs$; dotted lines: $\lambda_d = 1.2\ Vs$ (strong cross-saturation)

TABLE III
SUGGESTED TUNING PROCEDURE

	open loop	HF injection
Test #1	Evaluate a_{d0} and a_{dd} (Fig. 12)	Not necessary
Test #2	Evaluate L_q for tuning the HF tracking loop	Evaluate a_{q0} and a_{qq} (Fig. 13)
Test #3	Evaluate a_{dq} (Fig. 12)	Not necessary

speed range. The HF pulsating voltage (833 Hz) is injected along the estimated $\widehat{d}$ axis, while the $\widehat{q}$ HF current response is manipulated via the flux maps and used as error signal. Flux maps are therefore the key building block of this flux and position observer, even more at zero and low speed operation.

For this test, a slow triangular torque reference up to 21 Nm (150% of the rated value) was imposed to the machine when torque controlled. A driving machine imposed zero speed and a torque meter accurately measured the shaft torque. The test
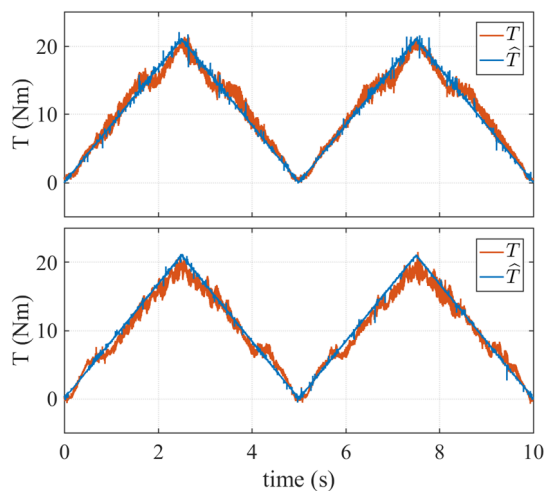
Fig. 14. Torque control tests using reference flux maps (upper) and the flux maps obtained with the proposed self commissioning augmented with HF injection (lower). Blue: observed torque; Orange: measured torque

was repeated two times: first using the reference flux maps and then using the saturation characteristics obtained from the self-commissioning augmented by HF injection. As can be seen in Fig. 14, thanks to the closed loop torque control the observed $\widehat{T}$ follows very well the reference. The measured T presets small irregularity at specific torque levels due to the slot-teeth interaction occurring at zero speed. Since the flux maps do not take into account slot harmonics, as common for sensorless control, the $\widehat{T}$ cannot track this phenomenon, explaining the small deviation. The torque tests obtained with the two methods are strictly compatible, proving the validity of the self-identification technique.

VI. CONCLUSION

The flux map identification proposed in [12] was augmented by introducing a position sensorless tracking loop that involves HF voltage injection at half of the switching frequency. This allowed to extend the measurement range and stability of test #2, where the q-axis saturation characteristic is evaluated. A slight improvement of the measurement area of test #3 (cross-saturation effect) was also achieved, but without significant effect on the obtained flux characteristic. Moreover, the flux error introduced by eventual inaccuracy in stator resistance estimation and compensation of inverter non-linear effects was analyzed and quantified. LLS procedure was used to obtain the parameters of a simple but accurate algebraic model, both for the tests with and without HF position tracking loop. Finally, the flux maps obtained in the two cases were used to implement a sensorless control of the motor under test, proving the goodness of the method and its validity for sensorless control in industrial applications.

REFERENCES

[1] Tuovinen, T.; Hinkkanen, M., "Adaptive Full-Order Observer With High-Frequency Signal Injection for Synchronous Reluctance Motor Drives," in *Emerging and Selected Topics in Power Electronics, IEEE Journal of,* vol.2, no.2, pp.181-189, June 2014.

[2] Agarlita, S. C.; Boldea, I.; Blaabjerg, F., "High-Frequency-Injection-Assisted Active-Flux-Based Sensorless Vector Control of Reluctance Synchronous Motors, With Experiments From Zero Speed," in *Industry Applications, IEEE Transactions on* , vol.48, no.6, pp.1931-1939, Nov.-Dec. 2012

[3] Foo, G.; Sayeef, S.; Rahman, M.F., "Low-Speed and Standstill Operation of a Sensorless Direct Torque and Flux Controlled IPM Synchronous Motor Drive," in Energy Conversion, IEEE Transactions on , vol.25, no.1, pp.25-33, March 2010.

[4] E. Armando, R. I. Bojoi, P. Guglielmi, G. Pellegrino and M. Pastorelli, "Experimental Identification of the Magnetic Model of Synchronous Machines," in *IEEE Transactions on Industry Applications*, vol. 49, no. 5, pp. 2116-2125, Sept.-Oct. 2013.

[5] L. Peretti, P. Sandulescu and G. Zanuso, "Self-commissioning of flux linkage curves of synchronous reluctance machines in quasi-standstill condition," in *IET Electric Power Applications*, vol. 9, no. 9, pp. 642-651, 11 2015.

[6] S. A. Odhano, R. Bojoi, . G. Rou and A. Tenconi, "Identification of the Magnetic Model of Permanent-Magnet Synchronous Machines Using DC-Biased Low-Frequency AC Signal Injection," in *IEEE Transactions on Industry Applications*, vol. 51, no. 4, pp. 3208-3215, July-Aug. 2015.

[7] D. Uzel and Z. Peroutka, "Optimal control and identification of model parameters of traction interior permanent magnet synchronous motor drive," in *Proc. IEEE IECON 2011*, Melbourne, Australia, Nov. 2011.

[8] S. Ebersberger and B. Piepenbreier, "Identification of differential inductances of permanent magnet synchronous machines using test current signal injection," in *Proc. SPEEDAM 2012*, Sorrento, Italy, June 2012, pp. 13421347.

[9] I. Omrane, E. Etien, O. Bachelier, and W. Dib, "A simplified least squares identification of permanent magnet synchronous motor parameters at standstill," in *Proc. IEEE IECON 2013*, Vienna, Austria, Nov. 2013

[10] B. Stumberger, G. Stumberger, D. Dolinar, A. Hamler and M. Trlep, "Evaluation of saturation and cross-magnetization effects in interior permanent-magnet synchronous motor," in *IEEE Transactions on Industry Applications*, vol. 39, no. 5, pp. 1264-1271, Sept.-Oct. 2003.

[11] N. Bedetti, S. Calligaro and R. Petrella, "Stand-Still Self-Identification of Flux Characteristics for Synchronous Reluctance Machines Using Novel Saturation Approximating Function and Multiple Linear Regression," in *IEEE Transactions on Industry Applications*, vol. 52, no. 4, pp. 3083-3092, July-Aug. 2016.

[12] M. Hinkkanen, P. Pescetto, E. Mölsä, S. E. Saarakkala, G. Pellegrino and R. Bojoi, "Sensorless Self-Commissioning of Synchronous Reluctance Motors at Standstill Without Rotor Locking," in *IEEE Transactions on Industry Applications,* vol. 53, no. 3, pp. 2120-2129, May-June 2017.

[13] P. Pescetto and G. Pellegrino, "Sensorless Commissioning of Synchronous Reluctance Machines Augmented with High Frequency Voltage Injection," *2017 IEEE Energy Conversion Congress and Expo (ECCE)*, Cincinnaty, Oh, 2017.

[14] Y. D. Yoon, S. K. Sul, S. Morimoto and K. Ide, "High-Bandwidth Sensorless Algorithm for AC Machines Based on Square-Wave-Type Voltage Injection," in *IEEE Transactions on Industry Applications*, vol. 47, no. 3, pp. 1361-1370, May-June 2011.

[15] P. Guglielmi, M. Pastorelli and A. Vagati, "Impact of cross-saturation in sensorless control of transverse-laminated synchronous reluctance motors," in *IEEE Transactions on Industrial Electronics*, vol. 53, no. 2, pp. 429-439, April 2006.

[16] A. Yousefi-Talouki; P. Pescetto; G. Pellegrino; I. Boldea, "Combined Active Flux and High Frequency Injection Methods for Sensorless Direct Flux Vector Control of Synchronous Reluctance Machines," in *IEEE Transactions on Power Electronics* , vol.PP, no.99, pp.1-1.

[17] P. Pescetto and G. Pellegrino, "Sensorless standstill commissioning of synchronous reluctance machines with automatic tuning," *2017 IEEE International Electric Machines and Drives Conference (IEMDC)*, Miami, FL, 2017, pp. 1-8.

[18] S. Bolognani and M. Zigliotto, "Self-commissioning compensation of inverter non-idealities for sensorless AC drives applications," *2002 International Conference on Power Electronics, Machines and Drives (Conf. Publ. No. 487)*, 2002, pp. 30-37.